Low Hydrogen Solubility in Clay Interlayers Limits Gas Loss in Hydrogen Geological Storage

SCHOLARONE™
Manuscripts

Low Hydrogen Solubility in Clay Interlayers Limits Gas Loss in Hydrogen Geological Storage

Tuan A. Ho[1*], Carlos F. Jove-Colon[2], and Yifeng Wang[2]

[1]*Geochemistry Department, Sandia National Laboratories, Albuquerque, NM 87185, USA*
[2]*Nuclear Waste Disposal Research and Analysis Department, Sandia National Laboratories, Albuquerque, NM 87185, USA*
Corresponding author: taho@sandia.gov

Abstract

Gas intercalation into clay interlayers may result in hydrogen loss in the geological storage of hydrogen; a phenomenon that has not been fully understood and quantified. Here we use metadynamics molecular simulations to calculate the free energy landscape of H_2 intercalation into montmorillonite interlayers and the H_2 solubility in the confined interlayer water; in comparison with results obtained for CO_2. The calculation results indicate that H_2 intercalation into hydrated interlayers is thermodynamically unfavorable while CO_2 intercalation can be favorable. H_2 solubility in hydrated clay interlayers is in the same order of magnitude as that in bulk water and therefore no over-solubility effect due to nanoconfinement is observed – in striking contrast with CO_2. These results indicate that H_2 loss and leakage through hydrated interlayers due to intercalation in a subsurface storage system, if any, is limited.

Hydrogen, a clean fuel that releases only water and heat upon combustion, is potentially a mitigating solution to anthropogenic greenhouse gas emission and climate change. H_2 produced from water electrolysis utilizing green energy is a zero-carbon energy carrier. Likewise, H_2 produced from hydrocarbon reformation is considered a low-carbon carrier if the by-product CO_2 is captured during production.[1] To enable a hydrogen economy, the H_2 supply chain from production, storage, and delivery to its end use needs to reach a higher technological readiness level. At present, surface H_2 storage technologies are relatively mature but limited by the H_2's low volumetric density (0.0838 kg.m^{-3} at 1 atm and 20°C).[2] Massive hydrogen geological storage (HGS) in depleted oil/gas/aquifer reservoirs or salt-caverns can potentially be a critical component of the hydrogen supply chain if H_2 is set to replace hydrocarbons to meet rising global energy demands.

When injected into a geological porous reservoir, H_2 interacts with earth materials (EMs) leading to various changes in mineral wettability,[3] gas solubility,[4] reservoir stress state, fluid transport properties of ambient rocks, thermo-physical properties of hydrogen interactions with other gaseous species,[5] and microbial activities[2] that may affect the technical and economic feasibility of HGS.[6] Recent experimental results indicate little risk of hydrogen loss or reservoir integrity degradation due to abiotic geochemical reactions in sandstone reservoirs.[7, 8] However, H_2 can be rapidly consumed[9] and transformed either into H_2S, formate, and methane[10] through

microbially mediated processes in subsurface environments, as confirmed by multiple studies of stored town gas. [11, 12]

This work focuses on hydrogen intercalation into phyllosilicates under relevant reservoir conditions; an important process that remains poorly investigated but may impact the performance of a HGS system. Phyllosilicates, which include clays, are one of the dominant mineral groups in both oil/gas reservoir rock and reservoir caprocks. H_2 intercalation into the interlayers of these minerals may directly contribute to a possible H_2 loss of a HGS system as well as the caprock integrity since H_2 uptake may cause changes in the mechanical properties of rock.[13, 14] H_2 intercalation into clay interlayers may also find its importance in deep geological nuclear waste repository concepts, where H_2 can be generated from metal corrosion of nuclear waste canisters. H_2 uptake and transport across a clay-based engineered barrier system is an important process that needs to be considered for nuclear waste disposal.[15-17]

Significant effort has been made to understand CO_2 intercalation into expansive clay interlayers.[18] Compared to a CO_2 molecule, a H_2 molecule is smaller (kinetic diameters of H_2 and CO_2 are 2.89 and 3.30 Å,[19] respectively). The quadrupole moment (13.4×10^{-40} C m^2) and polarizability (26.3×10^{-25} cm^3) of CO_2 [20] are higher than those for H_2 (2.1×10^{-40} C m^2 and 0.729 x 10^{-25} cm^3).[21-23] For CO_2 geological sequestration, many studies have concluded that clay minerals can adsorb a considerable amount of CO_2.[24, 25] On the one hand, CO_2 adsorption in clay minerals may induce clay swelling that leads to closure of fractures in caprock, thus improving seal integrity. On the other hand, hydrated clay in contact with dry CO_2 might dehydrate,[26, 27] possibly leading to desiccation and crack formation that can potentially pose a risk for CO_2 leakage. For HGS, the main question is: How is H_2 intercalation different from that of CO_2 given the differences in the fundamental properties of these two gases?

To answer this question, we first use metadynamics molecular dynamics (MD) simulations in LAMMPS package[28] to compare the free energy of H_2 intercalation into hydrated clay interlayers with the free energy of H_2 dissolution in bulk water. A detailed analysis of the relationship between the free energy profile and the clay layer structure illustrates the effect of H_2-water-clay molecular interactions on the intercalation process. We then use large-scale MD simulations to compare the solubility of H_2 in water confined in clay interlayers with that in bulk water. Finally, we compare the results obtained for H_2 with those published previously for CO_2.[18] Our overall conclusion is that H_2 intercalation into hydrated clay interlayers is thermodynamically unfavorable, and H_2 solubility in the confined water in the interlayers is comparable with or less than H_2 solubility in bulk water. In contrast, CO_2 intercalation into clay interlayers can be thermodynamically favorable, and the amount of CO_2 accumulated in the same clay interlayers is about one to two orders of magnitude higher than the amount of H_2.

In Fig. 1A we present the system used to calculate the potential of mean force (PMF, i.e., the free energy landscape) of H_2 dissolution in bulk water. The system contains a H_2 molecule and bulk water (2025 molecules). The free energy landscape (Fig. 1B) of moving a H_2 molecule from gas phase into water is calculated using well-tempered metadynamics MD simulations [see ESI

for more details and evidence (Fig. S1) for the convergence of the free energy profile calculation, and for the comparison of the PMF profiles for 2025 and 5175 water molecules].[29, 30] We implement a SPC water model[31] and a 3-site H_2 model[32] which reproduces well the solubility of H_2 in water (see ESI and Fig. S2 for H_2 model selection). The results in Fig. 1 indicate that the free energy of H_2 dissolution in bulk water is ~2.3 kcal/mol (i.e., the difference in the free energy between position 3 and position 1, Fig. 1B) indicating that the dissolution process is highly unfavorable. For comparison, the dissolution of CO_2 molecule in bulk water (Fig. 1B, reproduced from our previous work[18]) is slightly unfavorable with a free energy of ~0.5 kcal/mol. The free energy profile for CO_2 also suggests that CO_2 molecule prefers to accumulate at the water/vacuum interface with a free energy of ~ -0.5 kcal/mol (i.e., the difference in the free energy between position 2 and position 1, Fig. 1B). The high polarizability of CO_2 molecule is responsible for the favorable accumulation of CO_2 at the water/vacuum interface. H_2 does not tend to accumulate at the water/vacuum interface due to its low polarizability.

The primary goal of this study is to understand H_2 intercalation into swelling clay, e.g., montmorillonite (MMT). In Fig. 2A, we provide a part of a simulation system used to calculate the free energy landscape of H_2 intercalation into hydrated clay interlayers (see ESI, Fig. S3 for the whole simulation system). This system includes a MMT layer where an octahedral (O) Al-centered sheet is sandwiched between two Si-centered tetrahedral (T) sheets (i.e., TOT structure). We substitute some Mg atoms for Al atoms in the octahedral sheet to create two types of charge distributions[18]: patch-wise and random (see ESI, Fig. S4). The structural charge is balanced by cations (Na^+) in the interlayers. Because the interlayer cations tend to adsorb water, MMT can swell to intercalate 1 (1W), 2 (2W), and more water layers. See ESI for more details about the method to construct the clay layer and the adopted force field. In particular, the interaction parameters between MMT and H_2 were obtained by matching the structure of H_2 in nanopores calculated from MD simulations and that estimated from *ab initio* calculations (Fig. S5).
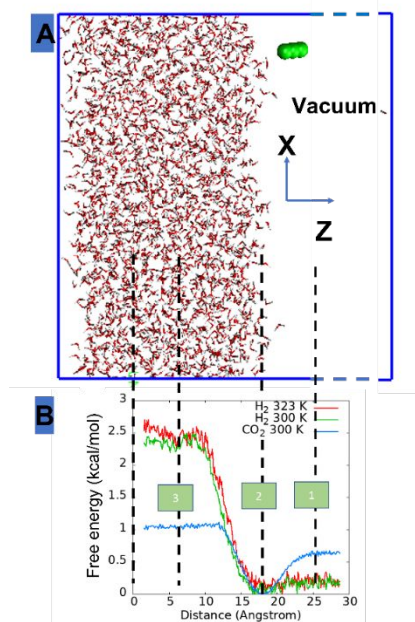
Figure 1. Simulation system (**A**) used to calculate the free energy landscape (**B**) of H_2 (green) dissolution in bulk water (red). The free energy profile is shown as a function of z positions of hydrogen molecule moving from vacuum (right) to bulk water (left). The molecular size is not to scale. There are 2025 water molecules and 1 H_2 molecule in a $50\times50\times70$ Å^3 simulation box. The free energy landscape of H_2 dissolution is compared with that of CO_2 dissolution reported in our previous work.[18] The black lines match the positions of gas molecule in the simulation box with the free energy profile.

During the PMF calculation, the H_2 molecule moves along the x direction, i.e., the reaction coordinate of the PMF is the x position of the H_2 molecule. The H_2 molecule is also restricted to move inside the blue region of the xy plane highlighted in Fig. 2B (see ESI and Fig. S6 for more details). Note that a PMF simulation can be run that allows the H_2 molecule to move to any position in the xy plane (e.g., no constraints in the y direction). However, there would be difficulties with correlating the PMF to the surface structure because its value would be averaged over a large heterogeneous surface, and more simulation time would be required for it to converge (see Fig. S7 for the convergence of the PMF calculation). The free energy for 2W hydrated interlayer is shown in Fig. 2C (red line). We also conduct the free energy calculation for 1W hydrated interlayer (Fig. 2D), and the result is shown in Fig. 2C (green line). For comparison, we reproduced the free energy profile for CO_2 (Fig. 2E) from our previous work.[18]

In its intercalation into a 2W interlayer (red line, Fig. 2C), the H_2 molecule has to move successively across the water/vacuum interface (position 1, Fig. 2C), the pore opening (position 2), and the hydrophobic domain (i.e., from position 2 to position 4; there is no charge substitution in the hydrophobic domain), before it finally enters the hydrophilic region (beyond position 4) with increasing charge density (i.e., an increasing number of Mg atoms in the blue region in Fig.

2B). Within the hydrophobic domain, the H_2 molecule experiences multiple minima (e.g., position 3, corresponding to the center of siloxane ring on the MMT surface) and maxima (e.g., position 4, corresponding to the rim of the siloxane ring). Overall, the free energy of H_2 accumulation at the minima (e.g., ~1.6 kcal/mol) is lower than the free energy of H_2 dissolution in bulk water (~2.3 kcal/mol), indicating that hydrophobic nanoconfinement enhances the H_2 accumulation at the siloxane ring center. Whereas in the hydrophilic region, the H_2 molecule experiences higher free energy (e.g., position 5) than it does in the hydrophobic region and also in bulk water. Overall, the H_2 intercalation into 2W interlayer is thermodynamically unfavorable with computed positive free energies. H_2 intercalation in the hydrophobic region is more favorable, compared to the intercalation into a hydrophilic region and dissolution in bulk water.

Reducing the interlayer d-spacing from 2W to 1W (green vs. red lines, Fig. 2C) doesn't seems to affect the intercalation in the hydrophobic region (e.g., the free energy at position 3 is comparable for 2W and 1W systems). However, this reduction seems to further inhibit the H_2 intercalation in the hydrophilic region (e.g., a higher free energy for 1W at position 5).

Through a comparison of the results for H_2 with those for CO_2 (Fig. 2E), many differences are observed. For example, CO_2 accumulation in the hydrophobic region (e.g., position 3) is thermodynamically favorable. Reducing the d-spacing from 2W to 1W enhances the CO_2 intercalation into the hydrophobic domain. The free energy of CO_2 accumulation in the hydrophilic region is lower than the H_2 accumulation free energy at the same position (e.g., position 5). The CO_2 molecule also prefers to accumulate at the water/air interface (position 1).

We can image the dissolution of gas molecule into bulk water/confined water as follow: a cavity with a size of a gas molecule is created in water and then a gas molecule is inserted into that cavity and interacts with other species around it.[18, 33, 34] Because the H_2 molecule is smaller than the CO_2 molecule, the energy required to create a H_2-size cavity is lower than that required to create a CO_2-size cavity. In addition, the probability of a cavity formation in the hydrophobic regions is higher than the probability to form a cavity in the hydrophilic regions.[35] In other words, due to its smaller size, H_2 would favor to dissolve in water, especially near hydrophobic surfaces. However, since the H_2 quadrupole moment and polarizability are much lower than those for the CO_2 molecule, H_2 interactions with other species are very weak thus hindering the H_2 molecule to dissolve in water. That is why H_2 dissolution in the hydrated clay nanopore is overall thermodynamically unfavorable; being less unfavorable in the hydrophobic region than in the hydrophilic region. Note that Na^+ ions concentrate in the hydrophilic region also contribute to the unfavorable intercalation (i.e., similar to the salting out effect in bulk solution). If we replace Na^+ by Ca^{2+} ion, the number of ions in the system would decrease and the interaction of water with Ca^{2+} would be stronger than that of water with Na^+, therefore the effect of counterions on the intercalation of H_2 need be investigated in a future study. Since CO_2 interactions with other components are stronger, CO_2

dissolution in bulk/confined water can be thermodynamically favorable, especially in the hydrophobic region.
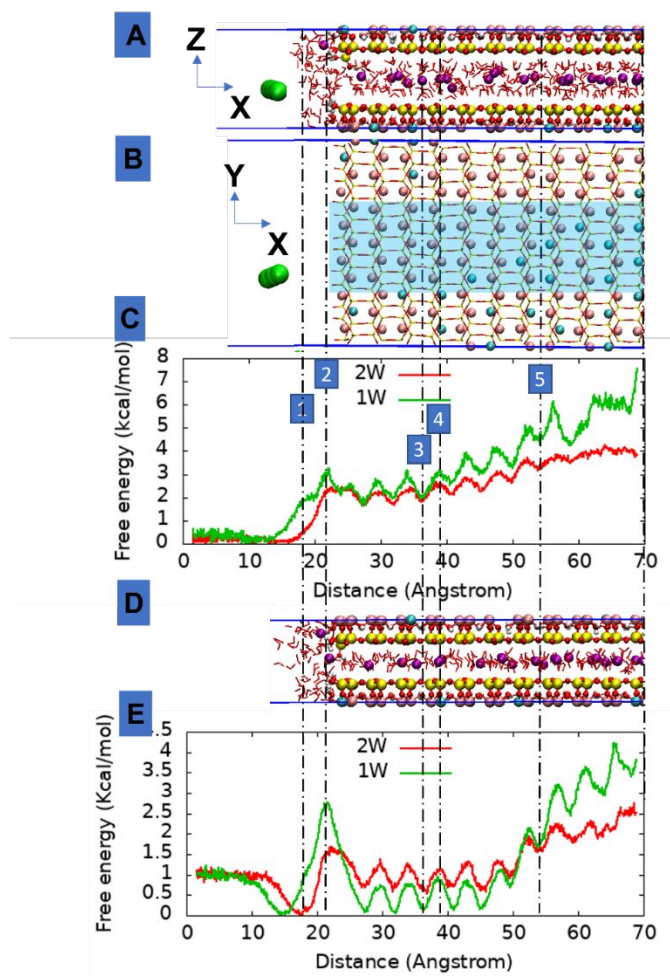
Figure 2. Side view of a part of the system used to calculate the free energy landscape of a hydrogen molecule (green) moving from vacuum into the 2W hydrated (water – red, Na^+ - purple) clay interlayer (**A**). Red, yellow, cyan, pink, and white are for O, Si, Mg, Al, and H of clay, respectively. The simulation box size is $200 \times 31.06 \times 15$ Å^3 (see ESI, Fig. S3 for full simulation system). Top view of the siloxane rings (red - yellow) and octahedral Al (pink) and Mg (cyan) atoms of clay layer (**B**). Charge distribution in Fig. 2B is patch-wise (see ESI, Fig. S4). During the PMF calculation, the hydrogen molecule is only allowed to move in the blue region highlighted in Fig. 2B. The free energy profiles for H_2 intercalation from vacuum into 1W (green) and 2W (red) hydrated clay interlayers at 323 K (**C**). The black lines match the structure of clay layer with the PMF profiles. Side view of the 1W hydrated clay system (**D**); the simulation box size is $200 \times 31.06 \times 12.5$ Å^3. d-spacing of interlayer is not allowed to change during the free energy calculation, i.e., d-spacing for 1W and 2W hydrated systems is fixed at 12.5 and 15 Å according to the experimental data.[36, 37] The free energy profiles for CO_2 intercalation (**E**). The molecular size is not to scale.
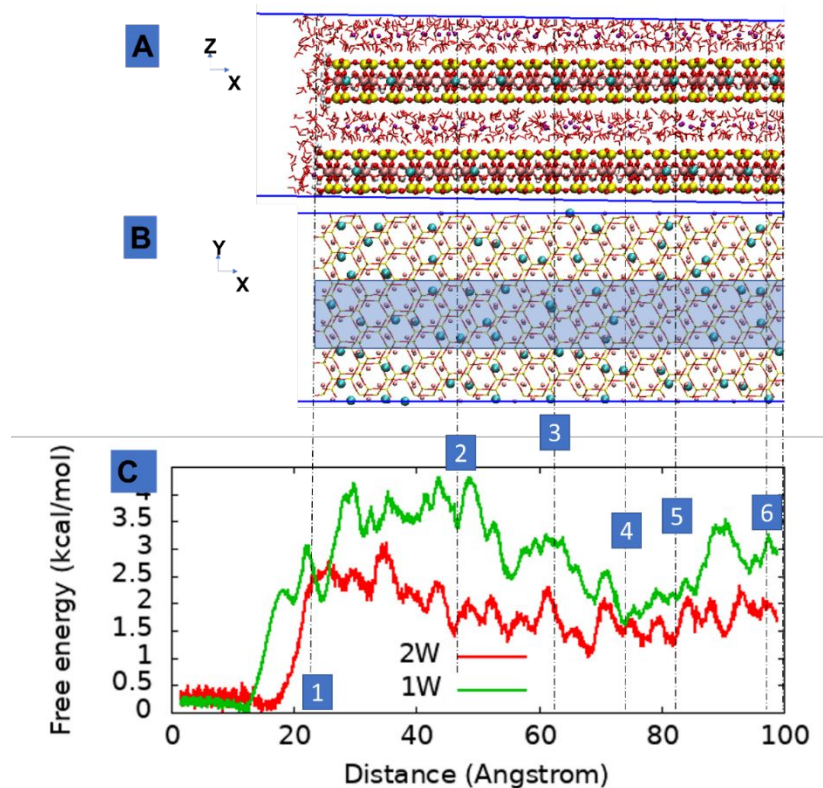
Figure 3. Side view of a complicated clay model used to calculate the free energy of a H_2 molecule moving from vacuum into the hydrated clay interlayer (**A**). The color code is similar with that in Fig. 2. Top view of the siloxane rings and octahedral Al and Mg atoms of clay layers that are above and below an interlayer (**B**). During the free energy calculation, the H_2 molecule is only allowed to move into the bottom pores, and within the blue shaded region in Fig. 3B. Free energy profile of a H_2 molecule moving from vacuum into 1W and 2W hydrated clay interlayer at 323 K (**C**). The black lines match the structure of clay layer with the PMF profile. The molecular size is not to scale. The convergence of the PMF profiles is reported in ESI, Fig. S8

The model in Fig. 2 is simple: water is confined between two identical clay layers with a patch-wise charge distribution. This means that when a gas molecule is in the hydrophobic/hydrophilic domain, it will experience hydrophobic/hydrophilic effects from both clay layers above and below it. In Fig. 3, we report the PMF results obtained from a more complicated clay model. The model in Fig. 3A includes two clay layers that form two interlayers when applying periodic boundary condition in the z direction. The charge distribution in each clay layer is random (e.g., Fig. 3B, and ESI, Fig. S4). There is a possibility that a hydrophobic domain exists above a gas molecule and a hydrophilic domain exists below that gas molecule. This asymmetry occurs in addition to the symmetric cases in which a gas molecule (and water) is confined between two hydrophobic domains, or between two hydrophilic domains (e.g., Fig. 2). The PMF calculation is carried out constraining the H_2 molecule to only enter the bottom pore.

The H_2 molecule is also restricted to move only in the blue region on the xy plane in Fig. 3B. The PMF in Fig. 3C suggests an alternating minima-maxima pattern on the PMF profile, where the minima are at the center of the siloxane rings (e.g., positions 2, 4, and 5) and the maxima are at the rim of the rings (e.g., positions 3 and 6). Even though the charge distribution in each layer is random, we can still observe a small hydrophobic domain (with the size of about a few siloxane rings near position 4 and 5) that reduces the free energy of H_2 intercalation for both 2W and 1W when compared to the free energy of H_2 intercalation at other locations. Reducing the interlayer d-spacing from 2W to 1W (green vs. red lines, Fig. 3C) seems to further inhibit H_2 intercalation.
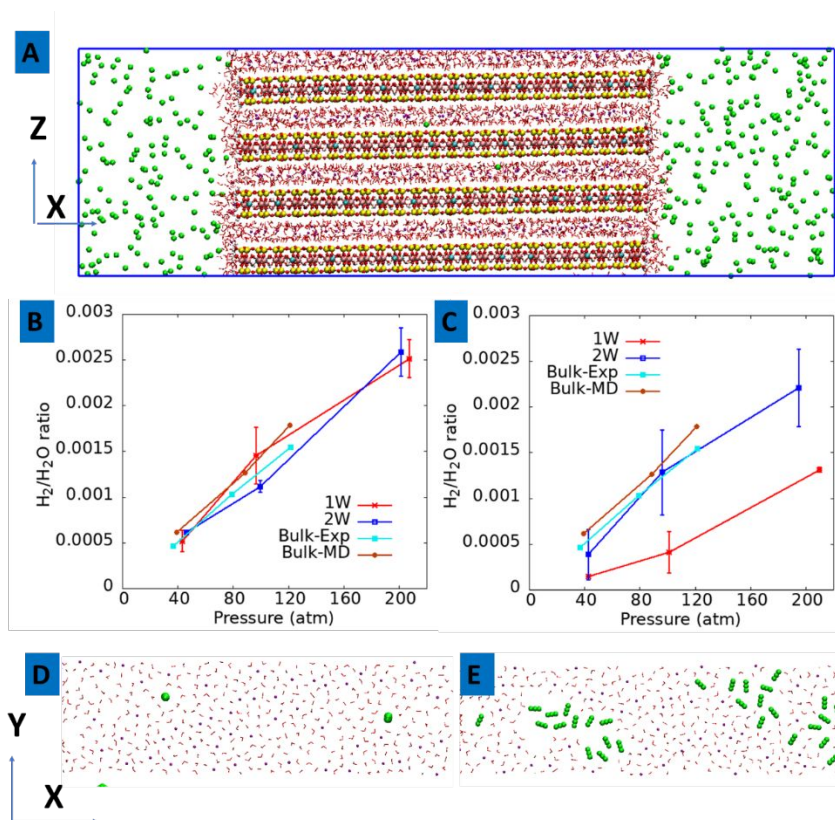
Figure 4. Simulation system (**A**) used to calculate H_2 solubility in water confined in clay interlayers. The simulation box size is $200 \times 31.06 \times 60$ Å^3. There are 11664 clay atoms, 2888 water molecules, and 208 Na$^+$ ions. The number of H_2 molecules depends on pressure. The pressure is determined based on the density of H_2 in the region outside the hydrated clay structure. H_2/H_2O ratio inside the interlayers for patch-wise (**B**) and random (**C**) charge distributions. These results are compared with experimental data (cyan line) from reference[4] and our MD data for bulk water (see also Fig. S2 in ESI for a good agreement between our MD data and experimental results for bulk water). Top (xy) view of intercalated H_2 (**D**) and CO_2 (**E**) with water and Na$^+$ ions in an 1W interlayer with patch-wise charge distribution. H_2 pressure for simulation of Fig. D is 207 atm, and CO_2 pressure for simulation of Fig. E is 61 atm.

The free energy results in Fig. 2 and 3 suggest that H_2 accumulation near hydrophobic sites is less unfavorable than H_2 accumulation near hydrophilic sites. The actual amount of H_2 intercalated will be the average of the effect of hydrophobicity/hydrophilicity and gas pressure. In our PMF simulation we only use one H_2 molecule. Because hydrogen can be considered as an ideal gas at a high pressure (i.e., H_2 - H_2 interaction can be ignored) adding more hydrogen molecules into the gas phase will not have a significant effect on free energy of inserting H_2 into water. To demonstrate this point we performed the PMF calculation for inserting a H_2 gas molecule from a 110 atm H_2 phase into bulk water and reported the PMF results in Fig. S9. Increasing H_2 pressure improves the convergence of the PMF profile, especially in the gas phase. However, little effect is observed for the free energy of inserting the H_2 into the water phase, i.e., the free energy is about 2.3 kcal/mol at 300K, which is the same with that reported in Fig. 1. This value also agrees with many experimental and theory results.[38, 39] Our results are also consistent with the fact that pressure has little effect on the Henry constant. To determine the amount of H_2 intercalated in the interlayers as a function of gas pressure we use the model depicted in Fig. 4A. Hydrogen molecules can enter the interlayers through the edges in the x direction during the MD simulation (NVT ensemble) at a temperature of 323 K, relevant to subsurface storage conditions. The simulation in Fig. 4A is conducted until the amount of H_2 in the interlayers reaches a constant value (e.g., 100 ns). The amount of H_2 in the interlayers as a function of H_2 pressure is reported in Fig. 4B and C for both patch-wise and random charge distributions, respectively. The results indicate that the H_2/H_2O ratio in interlayers is comparable or smaller than the ratio in bulk water. Relative to CO_2 (see Fig. S10), the amount of H_2 found in the interlayers is one to two orders of magnitude smaller. Our results also suggest that while CO_2 forms cluster and dries out water in the hydrophobic region, H_2 rarely forms a cluster in the interlayers even in the hydrophobic regions (Fig. 4D and E). Note that the dehydration[26, 27] due to CO_2 cluster formations potentially poses a risk for CO_2 leakage. Since H_2 cluster formation is not observed in the interlayers, the risk for H_2 leakage can be much lower.

In summary, we have used metadynamics molecular simulations to investigate the free energy landscape of H_2 intercalation into hydrated clay interlayers. The results indicate that H_2 intercalation is thermodynamically unfavorable. H_2 accumulation near hydrophobic sites is less unfavorable than accumulation near hydrophilic sites. H_2 solubility in confined water in the interlayers of swelling clay is comparable with H_2 solubility in pure water. Compared to CO_2, the amount of H_2 intercalated into hydrated interlayers is one to two orders of magnitude smaller. These results imply that in HGS H_2 loss due to adsorption into clay-rich caprock and leak through interlayers, if any, might be limited. Regarding the role of H_2 intercalation into clay interlayers in an engineered barrier system (EBS) in a nuclear waste repository, the results herein imply that H_2 pressure build up at the canister/EBS interface can be significant as H_2 intercalation is thermodynamically unfavorable and limited by water in the interlayers. Note that the research conducted here is for hydrated clay, either 1W or 2W. In a deep geological nuclear waste

repository, the EBS can be dry or partially saturated given the elevated thermal loads generated by the waste. Recent measurements of H_2 adsorption onto dry clay minerals[40] serves as a good starting point for our future calculation of H_2 intercalation and transport through partially wet/dry interlayers. Future research will also focus on comparison of H_2 and CH_4 adsorption/intercalation into clay interlayers because of potential H_2 storage in deleted natural gas reservoir.

Conflicts of interest

There are no conflicts to declare

Acknowledgements

Electronic supplementary information (ESI) available:

References

1. Hassanpouryouzband, A.; Joonaki, E.; Edlmann, K.; Haszeldine, R. S. *ACS Energy Letters* **2021,** 6, (6), 2181-2186.
2. Heinemann, N.; Alcalde, J.; Miocic, J. M.; Hangx, S. J. T.; Kallmeyer, J.; Ostertag-Henning, C.; Hassanpouryouzband, A.; Thaysen, E. M.; Strobel, G. J.; Schmidt-Hattenberger, C.; Edlmann, K.; Wilkinson, M.; Bentham, M.; Stuart Haszeldine, R.; Carbonell, R.; Rudloff, A. *Energy & Environmental Science* **2021,** 14, (2), 853-864.
3. Zeng, L.; Hosseini, M.; Keshavarz, A.; Iglauer, S.; Lu, Y.; Xie, Q. *International Journal of Hydrogen Energy* **2022,** 47, (60), 25357-25366.
4. Chabab, S.; Théveneau, P.; Coquelet, C.; Corvisier, J.; Paricaud, P. *International Journal of Hydrogen Energy* **2020,** 45, (56), 32206-32220.
5. Hassanpouryouzband, A.; Joonaki, E.; Edlmann, K.; Heinemann, N.; Yang, J. *Scientific Data* **2020,** 7, (1), 222.
6. Zivar, D.; Kumar, S.; Foroozesh, J. *International Journal of Hydrogen Energy* **2021,** 46, (45), 23436-23462.
7. Hassanpouryouzband, A.; Adie, K.; Cowen, T.; Thaysen, E. M.; Heinemann, N.; Butler, I. B.; Wilkinson, M.; Edlmann, K. *ACS Energy Letters* **2022,** 7, (7), 2203-2210.
8. Yekta, A. E.; Pichavant, M.; Audigane, P. *Applied Geochemistry* **2018,** 95, 182-194.

9.   Berta, M.; Dethlefsen, F.; Ebert, M.; Schäfer, D.; Dahmke, A. *Environmental Science & Technology* **2018,** 52, (8), 4937-4949.

10.   Haddad, P. G.; Ranchou-Peyruse, M.; Guignard, M.; Mura, J.; Casteran, F.; Ronjon-Magand, L.; Senechal, P.; Isaure, M. P.; Moonen, P.; Hoareau, G.; Dequidt, D.; Chiquet, P.; Caumette, G.; Cezac, P.; Ranchou-Peyruse, A. *Energy & Environmental Science* **2022,** 15, (8), 3400-3415.

11.   Šmigáň, P.; Greksák, M.; Kozánková, J.; Buzek, F.; Onderka, V.; Wolf, I. *FEMS Microbiology Letters* **1990,** 73, (3), 221-224.

12.   Buzek, F.; Onderka, V.; Vančura, P.; Wolf, I. *Fuel* **1994,** 73, (5), 747-752.

13.   Truche, L.; Joubert, G.; Dargent, M.; Martz, P.; Cathelineau, M.; Rigaudier, T.; Quirt, D. *Earth and Planetary Science Letters* **2018,** 493, 186-197.

14.   Didier, M.; Leone, L.; Greneche, J.-M.; Giffaut, E.; Charlet, L. *Environmental Science & Technology* **2012,** 46, (6), 3574-3579.

15.   Faybishenko, B.; Wang, Y.; Harrington, J.; Tamayo-Mas, E.; Birkholzer, J.; Jové-Colón, C. *Transport in Porous Media* **2022,** 141, (2), 585-606.

16.   Shaw, R. P.; Shaw, R. P., The Fate of Repository Gases (FORGE) project. In *Gas Generation and Migration in Deep Geological Radioactive Waste Repositories*, Geological Society of London: 2015; Vol. 415, p 0.

17.   Bardelli, F.; Mondelli, C.; Didier, M.; Vitillo, J. G.; Cavicchia, D. R.; Robinet, J.-C.; Leone, L.; Charlet, L. *Applied Geochemistry* **2014,** 49, 168-177.

18.   Ho, T. A.; Wang, Y.; Rempe, S. B.; Dasgupta, N.; Johnston, C. T.; Xu, G.; Zwier, T. S.; Mills, M. *The Journal of Physical Chemistry Letters* **2023,** 10.1021/acs.jpclett.3c00291.

19.   Kentish, E. S.; Scholes, A. C.; Stevens, W. G. *Recent Patents on Chemical Engineering* **2008,** 1, (1), 52-66.

20.   Walczak, R.; Savateev, A.; Heske, J.; Tarakina, N. V.; Sahoo, S.; Epping, J. D.; Kühne, T. D.; Kurpil, B.; Antonietti, M.; Oschatz, M. *Sustainable Energy & Fuels* **2019,** 3, (10), 2819-2827.

21.   Israelachvili, J. N., *Intermolecular and surface forces*. Academic Press: New York, 2011.

22.   Buckingham, A. D. *Quarterly Reviews, Chemical Society* **1959,** 13, (3), 183-214.

23.   Iglauer, S.; Abid, H.; Al-Yaseri, A.; Keshavarz, A. *Geophysical Research Letters* **2021,** 48, (10), e2021GL092976.

24.   Bowers, G. M.; Schaef, H. T.; Loring, J. S.; Hoyt, D. W.; Burton, S. D.; Walter, E. D.; Kirkpatrick, R. J. *The Journal of Physical Chemistry C* **2017,** 121, (1), 577-592.

25.   Busch, A.; Bertier, P.; Gensterblum, Y.; Rother, G.; Spiers, C. J.; Zhang, M.; Wentinck, H. M. *Geomechanics and Geophysics for Geo-Energy and Geo-Resources* **2016,** 2, (2), 111-130.

26.   Schaef, H. T.; Ilton, E. S.; Qafoku, O.; Martin, P. F.; Felmy, A. R.; Rosso, K. M. *Int. J. Greenh. Gas Control* **2012,** 6, 220-229.

27.   Schaef, H. T.; Loring, J. S.; Glezakou, V.-A.; Miller, Q. R. S.; Chen, J.; Owen, A. T.; Lee, M.-S.; Ilton, E. S.; Felmy, A. R.; McGrail, B. P.; Thompson, C. J. *Geochim Cosmochim Ac* **2015,** 161, 248-257.

28.   Plimpton, S. *J Comput Phys* **1995,** 117, (1), 1-19.

29.   Barducci, A.; Bussi, G.; Parrinello, M. *Phys Rev Lett* **2008,** 100, (2), 020603.

30.   Laio, A.; Parrinello, M. *Proceedings of the National Academy of Sciences* **2002,** 99, (20), 12562-12566.

31.   Teleman, O.; Jonsson, B.; Engstrom, S. *Mol Phys* **1987,** 60, (1), 193-203.

32.   Lopez-Lazaro, C.; Bachaud, P.; Moretti, I.; Ferrando, N. *Bulletin de la Société Géologique de France* **2019,** 190, (1).

33.   Baldwin, R. L. *Proceedings of the National Academy of Sciences* **2012,** 109, (19), 7310-7313.

34.   Pollack, G. L. *Science* **1991,** 251, (4999), 1323-1330.

35.   Godawat, R.; Jamadagni, S. N.; Garde, S. *Proceedings of the National Academy of Sciences* **2009,** 106, (36), 15119-15124.

36.   Tamura, K.; Yamada, H.; Nakazawa, H. *Clay Clay Miner* **2000,** 48, (3), 400-404.

37.   Ferrage, E.; Lanson, B.; Sakharov, B. A.; Drits, V. A. *American Mineralogist* **2005,** 90, (8-9), 1358-1374.

38.   Gadikota, G.; Dazas, B.; Rother, G.; Cheshire, M. C.; Bourg, I. C. *The Journal of Physical Chemistry C* **2017,** 121, (47), 26539-26550.

39.   Sabo, D.; Varma, S.; Martin, M. G.; Rempe, S. B. *The Journal of Physical Chemistry B* **2008,** 112, (3), 867-876.

40.   Ziemiański, P. P.; Derkowski, A. *International Journal of Hydrogen Energy* **2022,** 47, (67), 28794-28805.